Pak. J. Chem. 16(3):74-83, 2026 Research article
ISSN (Print): 2220-2625
ISSN (Online): 2222-307X DOI: 10.15228/2026.v16.i3.p08

Mg-Induced Structural Transitions and Blue-Shift in the Optical Properties of ZnO

Ramsha Saleem[1*], Humera Shaikh[1], Muhammad Saajan Bharhaam[2], Abdul Majid Soomro[1], Nek Muhammad Shaikh[1], Waseem Ahmed Bhutto[1], Irfan Ali Sanjrani[1], Zahid Hussain Arain[1], Muhammad Waseem Mirbhar[1], Tarique Ali Siyal[1], Naveed Abbas Nangraj[1]

[1]Institute of Physics, University of Sindh, Jamshoro, Pakistan

[2]Mehran University Institute of Science & Technology Development, Jamshoro, Pakistan

Corresponding Author email: taniramsha@gmail.com

Abstract

Mg-ZnO NPs with varying concentrations (4, 8, and 12) % were synthesized via a low-cost co-precipitation method. Morphological transition revealed by SEM: a significant change was observed in morphology due to the high temperature; NPs changed from irregular-shaped granules to spherical clusters for undoped ZnO to higher Mg concentrations. Single-phase hexagonal wurtzite structure confirmed by XRD in all samples, with peak shifts indicating the successful substitution of Zn^{2+} by Mg^{2+}. The Debye-Scherrer formula was used to find the average crystallite size; the particle size increased from 27.24nm to 31.19nm in the undoped ZnO and 12% Mg-doped samples, respectively, reflecting improved crystallinity. PL analysis demonstrated a significant blue shift in the Near Band Edge (NBE) emission, with the optical band-gap (calculated from the emission peak) increasing from 3.35 eV to 3.48 eV. EDX results validated the elemental purity of the Zn, O, and Mg constituents. The 8% Mg-ZnO sample showed the lowest PL intensity, indicating suppressed electron-hole recombination. These structural and optical modifications, particularly the formation of spherical clusters and the tuning of band gaps, make these Mg-ZnO NPs highly efficient candidates for the photocatalytic degradation of organic dyes in wastewater treatment.

Keywords: ZnO NPs, Mg doping, Co-precipitation, Blue shift

1. Introduction

Zinc oxide (ZnO) is a broadly used semiconductor material because of its remarkable physical [1] and chemical properties [2], including its 3.37eV wide direct band-gap [3], 60meV high exciton binding energy [4], and excellent chemical stability [5]. ZnO is a promising candidate for numerous applications such as photoelectronic devices [6], sensors, and energy-related systems [7]. Due to its low cost, non-toxicity, and ease of synthesis, it further enhances its technological significance [8]. To modify its functional properties for specific needs, ZnO is often tailored through doping [9]. Doping plays an important role in tailoring the electrical [10], structural [11], and optical [12] characteristics of ZnO by introducing controlled lattice defects and modifying its electronic band structure. Among many dopants, Al [13], Mn [14], Fe [15], Ni [16], Cu [17], Mg has obtained noticeable attention due to its similar ionic radius to Zn^{2+} and its ability to effectively substitute into the ZnO lattice without changing the fundamental hexagonal wurtzite structure [18]. Adding Mg^{2+} ions can alter the lattice structure and tune the band gap, leading to a blue shift of the absorption edge [19]. Such modification can lead to improved performance of ZnO-based materials in photocatalytic and UV-shielding applications [20]. A notable research gap remains in a wide-ranging study of Mg-doped ZnO [21]. Many studies focus on optical improvement without demonstrating a clear relation between high doping concentrations (up to 12%), induced lattice distortion, and the resulting morphological transitions [22]. In particular, systematic investigations linking these structural changes to defect-mediated Photoluminescence and band-gap tuning via the low-cost co-precipitation method remain limited [23]. In this context, the present study aims to systematically investigate the effect of varying Mg-doping concentrations (4, 8, and 12%) on the structural, morphological, and optical properties of ZnO nanoparticles [24]. To ensure the high crystallinity of the nanoparticles, thermal treatment plays an important role in removing residual moisture and organic impurities while providing the energy needed for proper atomic ordering of the lattice [25]. This leads to lower structural defects, a highly stable, well-defined crystal phase [26]. The novelty of this work lies in establishing a clear relationship between Mg-induced lattice modifications and the transition from hexagonal particles to spherical clusters [27]. It is hypothesized that the substitution of Zn^{2+} by Mg^{2+} ions will improve the crystalline quality and increase the crystallite size [28], leading to a significant widening of the band-gap (blue shift) [29]. Furthermore, this Mg incorporation into Zn is expected to optimize charge-carrier dynamics, thereby enhancing the material's potential for photocatalytic degradation of organic dyes in industrial wastewater remediation.

2.0. Materials and Methods

2.1. Chemical Reagents

All chemicals used in this study were of analytical grade and were used without further purification. Zinc chloride ($ZnCl_2$), magnesium chloride hexahydrate ($MgCl_2 \cdot 6H_2O$), sodium hydroxide (NaOH), and acetone (CH_3COCH_3) were purchased from Sigma-Aldrich. Deionized (DI) water was used for the preparation of all solutions.

2.2. Preparation of Stock Solutions

A 1.0 M zinc chloride ($ZnCl_2$) solution was prepared by dissolving the appropriate amount of $ZnCl_2$ in deionized water using a volumetric flask, followed by thorough stirring to ensure complete dissolution. Magnesium chloride hexahydrate ($MgCl_2 \cdot 6H_2O$) solutions at 4%, 8%, and 12% were similarly prepared in deionized water and used as dopant sources during the synthesis of ZnO nanoparticles. In addition, a 1.0 M sodium hydroxide (NaOH) solution was obtained by dissolving the required quantity of NaOH pellets in deionized water, with subsequent stirring and sonication to achieve complete dissolution

2.3. Synthesis of Undoped and Mg-Doped ZnO Nanoparticles

The co-precipitation method was applied for the synthesis of Undoped ZnO nanoparticles and Mg-doped ZnO nanoparticles (Fig. 1). A 1 M $ZnCl_2$ solution was placed in a clean 200 mL glass beaker and stirred using a magnetic stirrer. During stirring, a 1 M NaOH solution was added dropwise to the $ZnCl_2$ solution. The reaction mixture was maintained at approximately 50 °C and continuously stirred for about 1 hour. After completion of the reaction, the mixture was transferred to an oven and heated at 95 °C for 6 hours. During this process, $ZnCl_2$ is initially converted into $Zn(OH)_2$, which subsequently decomposes upon heating to form ZnO nanoparticles. The mixture was then cooled to room temperature, forming a visible precipitate. The precipitate was collected by filtration, washed several times with deionized water to remove impurities, and then washed with acetone. The obtained product was dried in an oven at 60 °C for 5 hours, followed by the same process of synthesis for Mg-doped ZnO nanoparticles. Appropriate amounts of $ZnCl_2$ and $MgCl_2$ solutions were mixed to achieve doping levels of 4%, 8%, and 12%. The co-precipitation process was carried out under identical conditions to ensure uniform incorporation of Mg^{2+} ions into the ZnO lattice. All samples were subsequently annealed under fixed conditions to improve crystallinity. The dried powders were placed in an alumina crucible and annealed isothermally in a resistance furnace from room temperature to 500 °C for 4 hours to obtain nanosized ZnO particles[31].

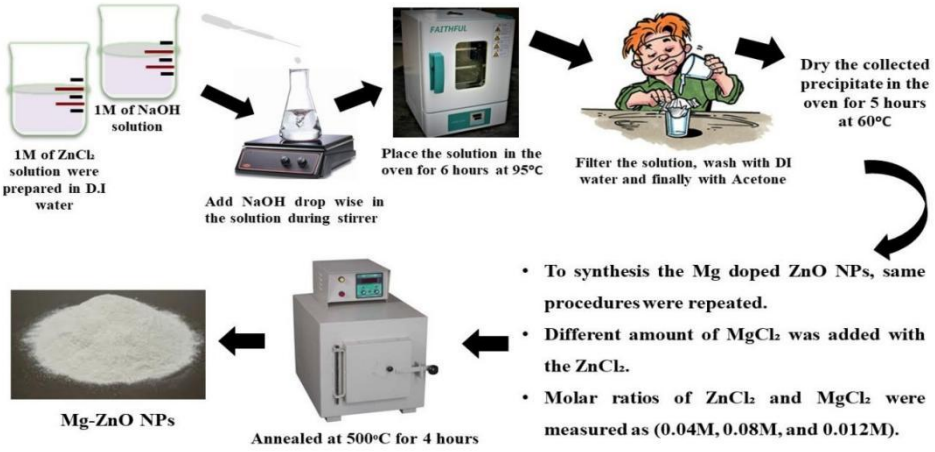

Figure 1: A schematic diagram shows the experimental procedure of Undoped ZnO and different concentrations of Mg content.

2.4. Structural Studies

Several characterized techniques examined Mg ZnO NPs. To analyze surface morphology, high- resolution images were acquired at an accelerating voltage of 10kV with a magnification of 10,000x. The structural studies of nanoparticles were characterized using a Panalytical X'Pert PRO diffractometer equipped with Cu-Kα radiation (1.5406 Å), operating at 40 kV and 40 mA. All measurements were conducted at room temperature to ensure the stability and accuracy of the results[32]. The measurements were taken over a 2θ range of 10° to 80°, with a scanning step size of 0.05 °. Optical properties were investigated by room-temperature photoluminescence spectroscopy with a PerkinElmer LS45 Fluorescence Spectrometer. The samples were tested at room temperature using an excitation wavelength in the UV range. The emission spectra were recorded from 300 nm to 700 nm with a scanning speed of 800 nm/min. The elemental composition of the nanoparticles was quantified using EDX spectroscopy.

3.0. Results and Discussion

The prepared nanostructures were characterized using advanced technologies and is discussed below.

3.1. Scanning Electron Microscope (SEM) of undoped ZnO and Mg-doped ZnO

Scanning Electron Microscopy (SEM) was used to examine the surface morphology and structure of the nanostructures. The SEM images of undoped ZnO and Mg-doped ZnO (4%, 8%, and 12%) are shown in Figure 2(a–d). From Figure 2(a), it can be seen that the undoped ZnO nanoparticles are irregularly shaped, granular, and have a relatively uniform distribution. These grains act as the building blocks for the hexagonal crystal lattice (confirmed by XRD).

After introducing Mg, noticeable changes in morphology occur. In Figures 2(b and c), corresponding to 4% and 8% Mg doping, the particle shape gradually shifts from granulated NPs to more spherical forms. In Figure 2(d), it is noted that

NPs tend to aggregate at higher concentration and form spherical clusters, which significantly influence the overall morphology and growth pattern as Mg content increases. Overall, the particles are slightly aggregated, which is due to the high-temperature annealing. This leads to an increase in particle size from 27.24nm to 31.19nm. This transition in size from small granules to spherical clusters is highly advantageous for photocatalytic dye degradation [33]. For dye adsorption, clustered morphology provides a stable surface [34]. While the inter-particle spaces within the clusters can enhance light trapping, ultimately improving the efficiency of organic pollutant removal in wastewater treatment [35].

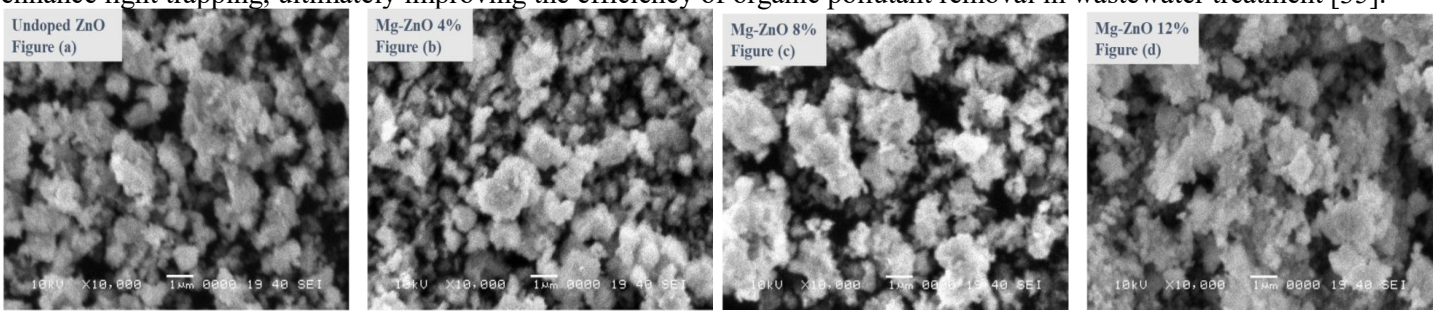

Figure 2: SEM images show the structural analysis of undoped and Mg-ZnO NPs. (a) undoped ZnO (b-d) 4%, 8%, 12% Mg-ZnO NPs respectively

3.2. Structural analysis through X-ray Diffraction (XRD)

The crystal structure of the NPs was analyzed by using X-ray diffraction (XRD). Figure 3(a–d) shows the XRD patterns of undoped ZnO and Mg-ZnO NPs (4, 8, and 12) %. All the XRD graphs exhibit a typical hexagonal wurtzite structure, confirming that the basic crystal structure of ZnO remains unchanged after doping. Seven prominent peaks are clearly observed at 31.6°, 34.3°, 36.1°, 47.4°, 56.5°, 62.8°, and 67.7°. These peaks correspond to the (100), (002), (101), (102), (110), (103), and (112) crystal planes, respectively, and match well with the standard JCPDS card No. 36-145 [6]. This rigorous structural confirmation supports the morphological observations seen in SEM, identifying the building blocks of the observed nanoparticles as wurtzite-phase ZnO [36]. This confirms the successful synthesis of undoped ZnO, with no secondary peaks. After Mg doping, no secondary peaks appear, which demonstrates their chemical purity and high crystalline quality. After doping, the peak positions shift slightly towards both lower and higher angles, indicating that Mg^{2+} ions are successfully replacing Zn^{2+} ions in the lattice. It is further noted that the peaks in the 8% and 12% Mg-doped samples shift toward higher angles. In comparison, the 4% doped sample shows a shift toward lower angles (Fig. 4). This difference is likely due to the strain or small defects introduced in the crystal structure as a result of Mg incorporation [37].

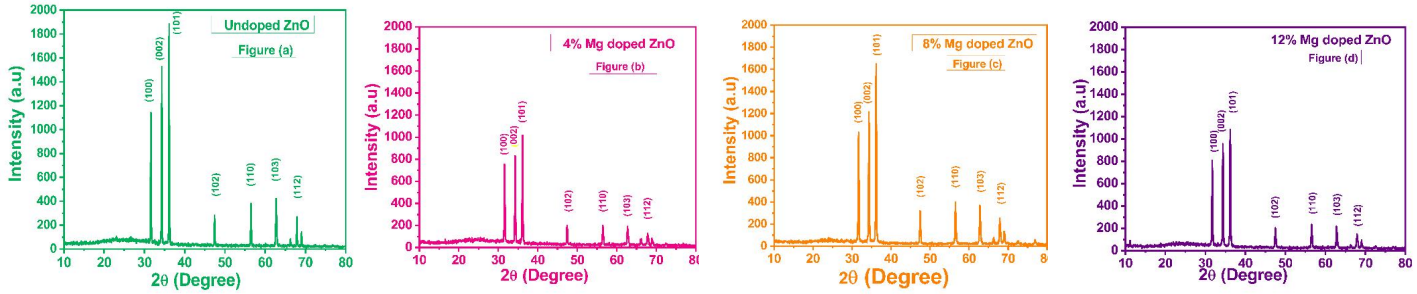

Figure 3: Depicts the XRD samples of Undoped and Mg-ZnO (a) Undoped (b) 4% (c) 8% (d) 12%

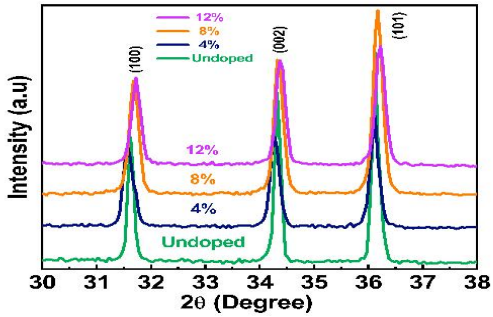

Figure 4: Major shift of Undoped and Mg-ZnO

The XRD patterns of samples annealed at 230 °C exhibit significant noise and the presence of secondary peaks (Fig. 5). To address this issue, the samples were re-annealed at 500 °C, resulting in a marked improvement in the diffraction patterns, as shown in Fig. 6. All samples exhibit a hexagonal wurtzite crystal structure (JCPDS card no. 36-1451) [38].

With increasing annealing temperature, the diffraction peaks become sharper and more intense, indicating enhanced crystallinity of the nanoparticles [39]. The observed decrease in the full width at half maximum (FWHM) of the diffraction peaks with increasing Mg content can be attributed to an increase in grain size [21]. No additional impurity or

secondary phases were detected upon Mg doping into the ZnO crystal lattice.The sample with 8% Mg content exhibits the highest peak intensity, suggesting superior crystalline quality, which is favorable for potential future applications.

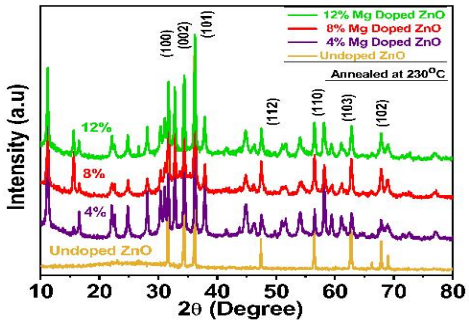

Figure 5: shows the multi XRD pattern of Undoped and Mg-ZnO samples annealed at 230°C

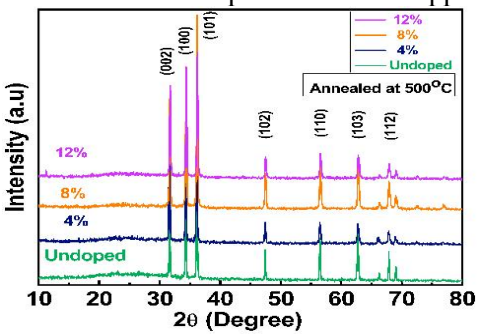

Figure 6: shows the multi XRD pattern of Undoped and Mg-ZnO samples annealed at 500°C

3.3. Mg Doping Effect on Crystallite Size

The Debye-Scherrer formula [40] was used to determine the crystallite size of undoped and Mg-ZnO NPs.

$$d = \frac{0.89\lambda}{\beta cos\theta}$$

Here, λ, β, and θ represent the wavelength of the X-ray radiation (1.54056 Å), the full width at half maximum (FWHM) of the peak, and the diffraction angle, respectively. Figure 7(a-c) illustrates the effect of Mg doping on the crystal structure of the nanoparticles, with detailed values given in Table 1. In Figure 7(a), the FWHM of the main diffraction peak gradually decreases from 0.277° to 0.242° as the Mg concentration increases upto 12%. This decrease indicates that the peaks are becoming sharper, suggesting better crystal quality and fewer structural defects [41]. Using the Scherer formula, the calculated average particle size (Table 1). For undoped ZnO, the particle size is 27.24 nm. With increasing Mg content, the final particle size is 31.19 nm, (Fig. 7b).The relationship between FWHM and crystallite size: as one parameter decreases, the other increases (Fig.7c). This inverse relationship suggests that adding Mg^{2+} ions helps the particles grow larger and become more well-ordered within this concentration range [42]. This structural improvement is vital for advancing the application of ZnO in environmental remediation, specifically for the photocatalytic degradation of organic dyes under natural sunlight irradiation [43]. By optimizing crystallite size and reducing structural defects, the charge-carrier recombination rate is effectively suppressed, thereby increasing the generation of reactive oxygen species, which are necessary for the rapid mineralization of toxic water pollutants [44].

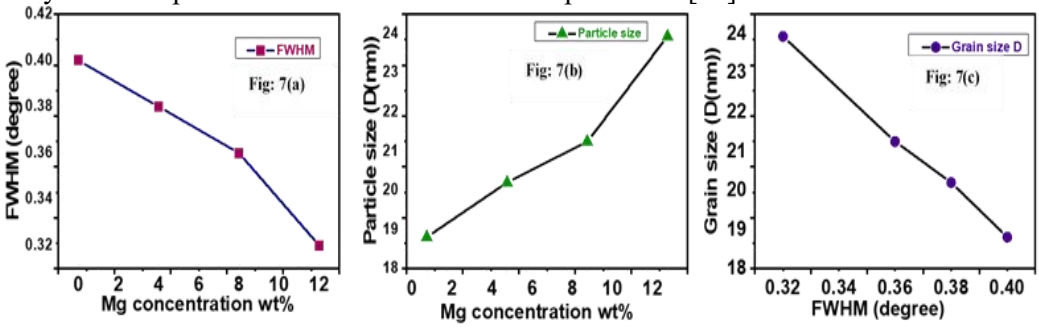

Figure 7(a-c): Illustrates the relationship between the Mg doping concentration and the crystalline evolution of NPs.

Table 1: Crystallite size of Undoped and Mg-ZnO NPs

Samples	2θ (Degree)	d-spacing (nm)	FWHM (Degree)	Crystallite size (D) nm
ZnO NPs	36.107	0.993	0.277	27.249
4% Mg-ZnO NPs	36.018	0.996	0.257	29.373
8% Mg-ZnO NPs	36.155	0.992	0.249	30.321
12% Mg ZnO NPs	36.203	0.991	0.242	31.199

3.4. Optical properties of Undoped ZnO and Mg-doped ZnO by Photoluminescence (PL) spectroscopy

For optimizing the optical properties of Undoped ZnO and Mg-doped ZnO samples, photoluminescence (PL) spectroscopy was used. The PL results arise from the recombination of photo-generated electrons and holes, which helps us understand how charges behave at the surface [45], how efficiently they are trapped, and how quickly they recombine [46]. The PL spectra for undoped ZnO and Mg-ZnO (4, 8, and 12) % is presented in the Figure 8.

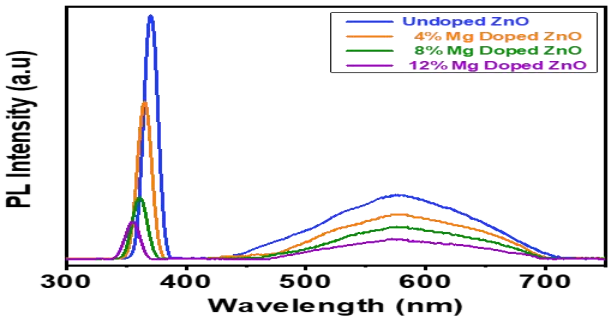

Figure 8: Photoluminescence spectra of Undoped and different Mg concentration with ZnO

Two main emission peaks are observed: one in the ultraviolet (UV) region, called the near-band-edge (NBE) [47], and the other in the visible region, known as deep-level emission (DLE) [48]. The NBE peak is related to direct recombination of electrons and holes (band-to-band transition), while the visible emission is mainly due to defects in the material [49]. At around 370nm, the UV emission peak appears for undoped ZnO, and for Mg-doped samples, shifts were observed at 365 nm, 361 nm, and 356 nm for 4%, 8%, and 12%, respectively (Table 2). This demonstrates an increase in band-gap energy from about 3.35eV to 3.48eV. The visible emission spans 430-715 nm, with a main peak at 577 nm (yellow-green). This emission is linked to structural defects [50]. However, its intensity decreases with increasing Mg content, which suggests that defects are being reduced [51]. There are many reasons for visible-region emission, which depend on the synthesis process, annealing temperature [52], doping material [53], pH parameters, and dopant concentration [54]. Another important observation is that the intensity of the NBE peak decreases as Mg concentration increases. This indicates reduced recombination of charge carriers and suggests better charge separation [20]. It also hints at an increase in particle size. Additionally, the peak becomes narrower, indicating that crystal quality improves as the Mg concentration increases. This is because of the annealing temperature (500^{O}C), which enhanced the crystal quality and increased the size of the Mg-ZnO NPs. Hence, it is observed that increasing the temperature leads to fewer defects, a better crystal structure, and an increased band gap [55]. These improvements enhance the optical properties of ZnO nanoparticles, making them more suitable for future applications, especially in photocatalysis [30].

Table 2: Band gap energy and wavelength of Undoped and Mg Concentration at (4, 8, 12) %

Composition	Wavelength (nm)	Band Gap Energy (eV)
Undoped	370	3.35
4% Mg doped ZnO	365	3.39
8% Mg doped ZnO	361	3.43
12% Mg doped ZnO	356	3.48

3.5. Band-gap analysis through Photoluminescence

The optical band gap (E_g) was estimated from the NBE emission peak position using the relation:
to address the optical behavior,

$$Eg = \frac{hc}{\lambda}$$

where "h" is Planck's constant, "c" is the speed of light, and "λ" is the emission wavelength. For undoped ZnO, the band-gap was calculated to be 3.35 eV. After the incorporation of Mg into ZnO, a systematic blue shift was observed in the NBE peak, with the band-gap increasing to 3.39eV, 3.43eV, and 3.48eV for the 4%, 8%, and 12% Mg samples, respectively (Fig. 9). This widening of the band-gap is attributed to the substitution of Zn^{2+} by Mg^{2+}, which modifies the electronic band structure [56].

3.6. Defect States and Photocatalytic Significance

A broad visible emission (green-yellow region) is observed in the UV spectrum, associated with intrinsic defects such as oxygen vacancies *(V_o)* and zinc interstitials *(Zn_i)*. Interestingly, the PL intensity decreases with increasing temperature and Mg doping up to 8%, suggesting a reduction in the electron-hole recombination rate. This suppression of recombination is a critical factor for photocatalytic dye degradation [57]. A lower recombination rate ensures that more photo-generated electrons and holes are available at the surfaces of spherical clusters to react with organic pollutants [58]. Therefore, the 8% Mg-doped sample, with its optimized band gap and reduced recombination, is expected to exhibit the highest efficiency in degrading industrial dyes under sunlight [1]. The increase in band-gap energy is crucial because, with Mg-doping, it reduces the recombination rate of photo-generated electrons and holes (Fig. 9) [59]. By reducing this recombination, more charge carriers remain available on the NPs surface to react with and break down organic pollutants [60]. Consequently, the 8% Mg-doped sample is identified as the most efficient for photocatalysis under sunlight due to this optimized balance of band-gap tuning and reduced defect-related recombination [59].

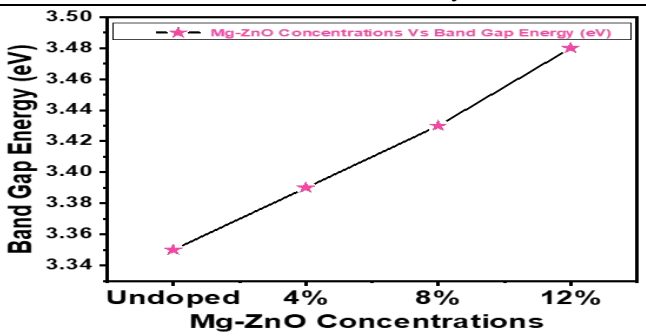

Figure 9: The relationship between Mg concentrations and band gap energy (eV) of ZnO NPs

3.7. EDX analysis for Undoped and Doped Mg-ZnO NPs

EDX was used to analyze the chemical composition of undoped ZnO and Mg-doped ZnO NPs to identify the percentage ratios of undoped ZnO and Mg-doped ZnO NPs, and to present only undoped ZnO and 8% Mg concentration in the EDX quantitative data. The weight and atomic percentages of elements in undoped and 8% Mg-ZnO NPs (Table 4). The elemental analysis confirms the formation of pure ZnO in the undoped sample, with Zn and O present in near-stoichiometric proportions. In the 8% Mg-doped ZnO, the appearance of Mg (3.15 wt%, 5.53 at%) verifies successful incorporation into the ZnO lattice. A slight decrease in Zn content indicates partial substitution of Zn^{2+} by Mg^{2+} ions. Additionally, the reduction in oxygen percentage suggests the possible formation of oxygen vacancies upon doping. Overall, the results confirm effective Mg doping with minor compositional changes in the ZnO structure.

Table 4: Shows the percentages of elements present in undoped and 8% Mg-ZnO NPs

Element	Wt% (undoped)	At% (undoped)	Wt% (8% Mg-ZnO)	At% (8% Mg- ZnO)
Zn	81.61	52.36	80.62	52.11
O	18.39	47.64	16.23	42.36
Mg	-	-	3.15	5.53

4.0 Conclusion

In this study, Mg-doped ZnO nanoparticles were successfully synthesized using a low-cost co-precipitation method with concentrations ranging from 0% to 12%. Annealing plays a crucial role in achieving high-crystal particles and NP aggregation. XRD analysis confirmed that all samples maintained a high-purity hexagonal wurtzite phase, with the average crystallite size increasing from 27.24 nm (undoped) to 31.19 nm (12% Mg). This incorporation of Mg^{2+} enhances the crystalline order and reduces lattice defects. SEM revealed a notable change in the NPs from irregular granular shapes to spherical clusters in the Undoped and Mg-doped samples. Optical studies using PL spectroscopy confirmed a blue shift in the near-band-edge emission, with the optical band gap widening from 3.35 eV to 3.48 eV. Notably, the 8% Mg-doped sample exhibited the most significant suppression of electron-hole recombination, as evidenced by the quenched PL intensity. This combination of an expanded band gap, improved crystallinity, and clustered morphologies suggests that these Mg-ZnO nanoparticles are highly effective for environmental remediation. Specifically, the optimized 8% sample shows great potential for photocatalytic degradation of organic dyes, offering a promising, sustainable solution for industrial wastewater treatment.

Acknowledgment

The Authors would like to thank the Institute of Physics at the University of Sindh for providing the facilities and technical support necessary to complete this research.

Author's Contribution:

Ramsha Saleem (Conceptualization, investigation, methodology, formal analysis, data curation, validation, writing original draft, and editing), Humera Shaikh (Investigation, data curation, validation, and editing), Muhammad Sajaan Bharhaam (editing and validation), Abdul Majid Soomro (Supervision, review, and validation), Waseem Ahmed Bhutto (Supervision, review, and validation), Nek Muhammad Shaikh (Supervision, review, and validation), Irfan Ali Sanjrani (Literature search), Zahid Hussain Arain (format of the article), Muhammad Waseem Mirbhar (Visualization), Tarique Ali Siyal (Visualization), Naveed Abbas Nangraj (facitilation)

Conflict of Interest: The authors have no conflict of interest.

Funding Resource: This research received no external funding.

References

1. Saleem, R., Shaikh, H., Barhaam, M. S., Shah, Q. A., Waryani, B., Abbasi, M. A., Halepoto, I. A., Shaikh, N. M., Bhatti, M. A., Ibrahim, R. M., Dawi, E., Tahira, A., Tonezzer, M., & Ibupoto, Z. H. (2026). Facile and Low Cost Synthesis of NiFe-LDH/ZnO Composites for Efficient Photodegradation of MB in Aqueous Solution Under the Illumination of Natural Sunlight. Water, Air, & Soil Pollution, 237(8), 504. https://doi.org/10.1007/s11270-026-09216-7

2. Djurišić, A. B., Chen, X., Leung, Y. H., & Man Ching Ng, A. (2012). ZnO nanostructures: growth{,} properties and applications. J. Mater. Chem., 22(14), 6526–6535. https://doi.org/10.1039/C2JM15548F
3. Sharma, D. K., Shukla, S., Sharma, K. K., & Kumar, V. (2022). A review on ZnO: Fundamental properties and applications. Materials Today: Proceedings, 49, 3028–3035. https://doi.org/https://doi.org/10.1016/j.matpr.2020.10.238
4. Coleman, V. A., & Jagadish, C. (2006). Chapter 1 - Basic Properties and Applications of ZnO (C. Jagadish & S. B. T.-Z. O. B. Pearton Thin Films and Nanostructures, Eds.; pp. 1–20). Elsevier Science Ltd. https://doi.org/https://doi.org/10.1016/B978-008044722-3/50001-4
5. Raha, S., & Ahmaruzzaman, M. (2022). ZnO nanostructured materials and their potential applications: progress{,} challenges and perspectives. Nanoscale Adv., 4(8), 1868–1925. https://doi.org/10.1039/D1NA00880C
6. Kangathara, N., Sabari, V., Saravanan, L., & Elangovan, S. (2022). Synthesis, Characterization, and Comparison of Pure Zinc Oxide and Magnesium-Doped Zinc Oxide Nanoparticles and their Application on Ethanol Sensing Activities. Journal of Nanomaterials, 2022(1), 1769278. https://doi.org/https://doi.org/10.1155/2022/1769278
7. Sabir, S., Arshad, M., & Chaudhari, S. K. (2014). Zinc Oxide Nanoparticles for Revolutionizing Agriculture: Synthesis and Applications. The Scientific World Journal, 2014, 925494. https://doi.org/10.1155/2014/925494
8. Habtemariam, T. H., Anjullo, S. H., & Abebe, G. M. (2026). Green synthesis and antibacterial activity of zinc oxide nanoparticles using Croton macrostachyus Hochst. ex Delile extracts. RSC Adv., 16(16), 14492–14508. https://doi.org/10.1039/D6RA00724D
9. Khataee, A., Kiranşan, M., Karaca, S., & Arefi-Oskoui, S. (2016). Preparation and characterization of ZnO/MMT nanocomposite for photocatalytic ozonation of a disperse dye. Turkish Journal of Chemistry, 40(4), 546–564. https://doi.org/10.3906/kim-1507-77
10. Saleh, N. B., Milliron, D. J., Aich, N., Katz, L. E., Liljestrand, H. M., & Kirisits, M. J. (2016). Importance of doping, dopant distribution, and defects on electronic band structure alteration of metal oxide nanoparticles: Implications for reactive oxygen species. Science of The Total Environment, 568, 926–932. https://doi.org/https://doi.org/10.1016/j.scitotenv.2016.06.145
11. Huang, Y., He, J., Zhang, Y., Dai, Y., Gu, Y., Wang, S., & Zhou, C. (2006). Morphology, structures and properties of ZnO nanobelts fabricated by Zn-powder evaporation without catalyst at lower temperature. Journal of Materials Science, 41(10), 3057–3062. https://doi.org/10.1007/s10853-006-6978-9
12. Bahamonde Soria, R., Estupiñan, J., Gonza, I., Naranjo, M., Chinchin-Piñan, B. D., Manangón, L. E., Vaca, K., Romero-Bastidas, M., Pupiales, H., Taco, V., & Luis, P. (2026). Enhancing Photocatalytic Performance of ZnO Nanoparticles Through Er/Al Co-Doping for Solar-Driven Environmental Remediation. Clean Technologies, 8(2). https://doi.org/10.3390/cleantechnol8020053
13. Moussa Tankari, A., Medjnoun, K., Nouiri, M., Briot, O., Juillaguet, S., Peyre, H., Belaqziz, M., & Djessas, K. (2023). Synthesis and characterization of aluminum doped zinc oxide nanoparticles via a novel and low cost aqueous chemical process. Materials Letters, 353, 135230. https://doi.org/https://doi.org/10.1016/j.matlet.2023.135230
14. Rahal, A., Bouchama, I., Ghebouli, M. A., Alanazi, F. K., Ghebouli, B., Fatmi, M., Chihi, T., Althagafi, T. M., & Khettab, K. (2025). Experimental investigation of structural and optical properties of Mn-doped ZnO thin films deposited by pneumatic spray technique. Scientific Reports, 15(1), 7086. https://doi.org/10.1038/s41598-025-90425-1
15. Imboon, T., Sugio, K., Khumphon, J., Sridawong, L., Mangala Gowri, V., Yamada, K., Shima, M., & Thongmee, S. (2025). Synergistic Effects of Fe-Doped ZnO and Graphene Oxide for Enhanced Photocatalytic Performance and Tunable Magnetic Properties. ACS Omega, 10(31), 34571–34587. https://doi.org/10.1021/acsomega.5c03213
16. P., S. S., Y., A., & Ramanaiah, M. (2025). Ni Doped ZnO Nanostructures: Synthesis, Characterization and It's Sensing Behaviour at Lower Concentration and High Temperature. ECS Journal of Solid State Science and Technology, 14(10), 107001. https://doi.org/10.1149/2162-8777/ae0964
17. Chen, G., Yang, M., Tian, B., Yao, J., Chen, S., Li, D., & Yuan, G. (2025). Cu-doped ZnO nanoparticles and its application for the photocatalytic degradation of Rhodamine B. Scientific Reports, 15(1), 18246. https://doi.org/10.1038/s41598-025-02432-x
18. El Beji, M., Hafiene, N., Jdir, M., Jaballah, S., Bessadok, M. N., Ben Ali, F., Neri, G., & El Mir, L. (2025). Development of magnesium-doped zinc oxide nanopowders for conductometric acetone gas sensors. RSC Advances, 15(48), 40368–40380. https://doi.org/10.1039/d5ra05067g
19. Anujency, M., Ibrahim, M. M., Vinoth, S., Jeffery, A. A., Balu, K., Kumar, M., Algarni, H., & Shkir, M. (2026). Dopant-induced structural modulation and enhanced photosensing response in Mn-doped ZnO nanoparticles prepared by co-precipitation. Materials Chemistry and Physics, 353, 132113. https://doi.org/https://doi.org/10.1016/j.matchemphys.2026.132113
20. Shaikh, H., Saleem, R., Halepoto, I. A., Barhaam, M. S., Soomro, M. Y., Abbasi, M. A., Shaikh, N. M., Bhatti, M. A., Wassan, S. H., Dawi, E., Tahira, A., Tonezzer, M., & Ibupoto, Z. H. (2025). Facile and Low-Cost Fabrication

of ZnO/Kaolinite Composites by Modifying the Kaolinite Composition for Efficient Degradation of Methylene Blue Under Sunlight Illumination. Catalysts, 15(6). https://doi.org/10.3390/catal15060566

21. Kaliyur Nanjundaiah, G., Hanumanthappa, S., & Rudrappa, S. (2026). The electrical, optical, and photocatalytic properties of Mg-doped ZnO nanoparticles synthesized via solution combustion. International Journal of Materials Research, 117(1), 36–47. https://doi.org/doi:10.1515/ijmr-2025-0027
22. Kumar, M., Kumar, A., Dabas, S., Negi, A. S., Gupta, K., Kumar, P., Gautam, R. K. S., Tripathi, V. M., Singh, M. K., & Sharma, S. (2026). Structural evolution and optical tailoring of Mg-doped ZnO: Insights into doping-induced modifications. Scientific Reports, 16(1), 8919. https://doi.org/10.1038/s41598-026-40403-y
23. Arshad, M., Meenhaz Ansari, M., Ahmed, A. S., Tripathi, P., Ashraf, S. S. Z., Naqvi, A. H., & Azam, A. (2015). Band gap engineering and enhanced Photoluminescence of Mg doped ZnO nanoparticles synthesized by wet chemical route. Journal of Luminescence, 161, 275–280. https://doi.org/https://doi.org/10.1016/j.jlumin.2014.12.016
24. Naseer, H., Al-Zaqri, N., Iqbal, T., Yousaf, M., Afsheen, S., Sultan, M. S., Warad, I., Farooq, M., & Masood, A. (2023). Investigation of Mg Doped ZnO Nanoparticles Decorated with Ag for Efficient Photocatalytic Degradation. Journal of Inorganic and Organometallic Polymers and Materials, 33(9), 2790–2802. https://doi.org/10.1007/s10904-023-02722-9
25. Kim, B., Lee, D., Hwang, B., Kim, D.-J., & Kim, C. K. (2022). Effects of Mg doping and annealing temperature on the performance of Mg-doped ZnO nanoparticle thin-film transistors. Molecular Crystals and Liquid Crystals, 735(1), 61–74. https://doi.org/10.1080/15421406.2021.1972229
26. Luo, J., Liu, H., Deng, W., Zhang, R., & He, C. (2024). The effect of Mg doping concentration and annealing on the structure and luminescence properties of ZnO thin films. Journal of Materials Science: Materials in Electronics, 35(11), 744. https://doi.org/10.1007/s10854-024-12520-9
27. Bappy, N. F., & Subramani, S. (2025). A comprehensive review on Mg-doped ZnO thin film and nanostructure: Properties and applications. Materials Science and Engineering: B, 318, 118251. https://doi.org/https://doi.org/10.1016/j.mseb.2025.118251
28. Rehman, F., Sabah, A., Khanam, S., Younis, U., & Mehmood, M. Q. (2023). Synthesis and Characterization of Magnesium doped Zinc Sulphide Nanoparticles to Study Optical Properties. 2023 20th International Bhurban Conference on Applied Sciences and Technology (IBCAST), 541–544. https://doi.org/10.1109/IBCAST59916.2023.10712901
29. Kumar, Y., Kumar, H., Rawat, G., Pal, B. N., & Jit, S. (2020). Mg Doping Effects on Optical and Electrical Properties of Solution-Processed ZnO Quantum Dots Based Thin Film Devices. 2020 6th International Conference on Signal Processing and Communication (ICSC), 240–242. https://doi.org/10.1109/ICSC48311.2020.9182747
30. Lim, N. Y. Y., Chiam, S. L., Leo, C. P., & Chang, C. K. (2024). Recent modification, mechanisms, and performance of zinc oxide-based photocatalysts for sustainable dye degradation. Hybrid Advances, 7, 100318. https://doi.org/https://doi.org/10.1016/j.hybadv.2024.100318
31. Malek, M. F., Mamat, M. H., Musa, M. Z., Khusaimi, Z., Sahdan, M. Z., Suriani, A. B., Ishak, A., Saurdi, I., Rahman, S. A., & Rusop, M. (2014). Thermal annealing-induced formation of ZnO nanoparticles: Minimum strain and stress ameliorate preferred c-axis orientation and crystal-growth properties. Journal of Alloys and Compounds, 610, 575–588. https://doi.org/https://doi.org/10.1016/j.jallcom.2014.05.036
32. Belo, F. A., Soares, M. B., Lima Filho, A. C., Lima, T. L. de V., & Adissi, M. O. (2023). Accuracy and Precision Improvement of Temperature Measurement Using Statistical Analysis/Central Limit Theorem. Sensors (Basel, Switzerland), 23(6). https://doi.org/10.3390/s23063210
33. Junploy, P., Janta, R., Wongchai, P., Thongtem, T., & Thongtem, S. (2021). Photodegradation of organic dyes and antibacterial activity of Escherichia coli and Staphylococcus aureus by ZnO nanoparticles under UVA radiation. Materials Technology, 00(00), 1–9. https://doi.org/10.1080/10667857.2021.1885226
34. Pushpa, M., Mageswari, S., Shereenaa, S. N., & Surendhiran, S. (2025). Facile Phyto fabrication of Mg interconnected ZrO2 nanocomposites for effective decontamination of infected water bodies. Journal of the Indian Chemical Society, 102(11), 102193. https://doi.org/https://doi.org/10.1016/j.jics.2025.102193
35. Ikram, M., Mahmood, A., Haider, A., Naz, S., Ul-Hamid, A., Nabgan, W., Shahzadi, I., Haider, J., Ahmad, I., & Ali, S. (2026). Corrigendum to "Dye degradation, antibacterial and in-silico analysis of Mg/cellulose-doped ZnO nanoparticles" [Int. J. Biol. Macromol. 185 (2021) 153-164]. In International journal of biological macromolecules (Vol. 337, Number Pt 2, p. 149911). https://doi.org/10.1016/j.ijbiomac.2025.149911
36. Selvam, P. P., Rathinam, V., Arunraj, A., Ali Baig, A. B., & Govindhan, M. (2023). Synthesis effect of Mg-doped ZnO nanoparticles for visible light photocatalysis. Ionics, 29(9), 3723–3729. https://doi.org/10.1007/s11581-023-05079-8
37. Ievtushenko, A., Karpyna, V., Myroniuk, L., Myroniuk, D., Petrosian, L., Olifan, O., Kolomys, O., & Strelchuk, V. (2024). Effect of magnesium doping on the structure, optical properties and photocatalytic efficiency of ZnO

nanostructures deposited by atmospheric pressure MOCVD. Chemical Physics Letters, 857, 141720. https://doi.org/https://doi.org/10.1016/j.cplett.2024.141720

38. Etacheri, V., Roshan, R., & Kumar, V. (2012). Mg-Doped ZnO Nanoparticles for Efficient Sunlight-Driven Photocatalysis. ACS Applied Materials & Interfaces, 4(5), 2717–2725. https://doi.org/10.1021/am300359h
39. Etcheverry, L. P., Flores, W. H., Silva, D. L. da, & Moreira, E. C. (2018). Annealing effects on the structural and optical properties of ZnO nanostructures. Materials Research, 21(2), 1–7. https://doi.org/10.1590/1980-5373-mr-2017-0936
40. Ghaneialvar, H., Soltani, L., Mami, S., Azizian, H., Abbasi, N., Gholami, M., Molaei, S., Ghadermazi, M., Alizadeh, R., Akbari, A. R., Yari, M., & Soltani, S. (2025). Green Synthesis of ZnO and Mg-doped ZnO Nanoparticles Using Ferulago angulata Plant Extract and Its Effect on Second-Degree Burn Wound Healing. Cell Biochemistry and Function, 43(9), e70121. https://doi.org/https://doi.org/10.1002/cbf.70121
41. Sagheer, R., Khalil, M., Abbas, V., Kayani, Z. N., Tariq, U., & Ashraf, F. (2020). Effect of Mg doping on structural, morphological, optical and thermal properties of ZnO nanoparticles. Optik, 200, 163428. https://api.semanticscholar.org/CorpusID:204207876
42. Jadhav, S. A., Lokhande, S. D., Umadevi, G., & Mote, V. D. (2025). Synthesis of Mg doped ZnO cauli-flower nanostructures using chemical spray and its investigation for ammonia gas sensing at room temperature. Talanta, 285, 127403. https://doi.org/https://doi.org/10.1016/j.talanta.2024.127403
43. Sanna, V., Pala, N., Alzari, V., Nuvoli, D., & Carcelli, M. (2016). ZnO nanoparticles with high degradation efficiency of organic dyes under sunlight irradiation. Materials Letters, 162, 257–260. https://doi.org/https://doi.org/10.1016/j.matlet.2015.10.031
44. Majeed, A., Iqbal, M. A., & Do, T.-O. (2025). Advances in Composite Photocatalysts for Efficient Degradation of Organic Pollutants: Strategies, Challenges, and Future Perspectives. In Catalysts (Vol. 15, Number 9, p. 893). https://doi.org/10.3390/catal15090893
45. Jogi, A., Ayana, A., & Rajendra, B. V. (2023). Modulation of optical and Photoluminescence properties of ZnO thin films by Mg dopant. Journal of Materials Science: Materials in Electronics, 34(7), 624. https://doi.org/10.1007/s10854-023-09999-z
46. Bezerra Neta, I. A., Andrade Neto, N. F., Silva, J. M. P., Teodoro, M. D., Bomio, M. R. D., & Motta, F. V. (2023). Photoluminescent and photocatalytic properties of Cu2+ and Mg2+-doped ZnO nanoparticles obtained by a facile sonochemical method. International Journal of Ceramic Engineering & Science, 5(6), e10192. https://doi.org/https://doi.org/10.1002/ces2.10192
47. Arda, L., Karatas, O., Alphan, M. C., & Ozugurlu, E. (2024). Electron spin resonance and photoluminescence studies of Co/Mg co-doped ZnO nanoparticles. International Journal of Applied Ceramic Technology, 21(3), 2458–2473. https://doi.org/https://doi.org/10.1111/ijac.14602
48. Malpani, M., Shekhawat, K., Chattopadhyay, S., Misra, R. D. K., & Misra, K. P. (2025). Defects induced Photoluminescence and alteration of band gap and morphology in Ca doped sol-gel co-precipitated ZnO nanoparticles. Discover Applied Sciences, 7(11), 1303. https://doi.org/10.1007/s42452-025-07816-2
49. Shan, F., Kim, B., Liu, G. X., Liu, Z., Sohn, J. Y., Lee, W. J., Shin, B. C., & Yu, Y. S. (2004). Blueshift of near band edge emission in Mg doped ZnO thin films and aging. Journal of Applied Physics, 95, 4772–4776. https://api.semanticscholar.org/CorpusID:121935513
50. Umaralikhan, L., & Jaffar, M. (2017). Green synthesis of ZnO and Mg doped ZnO nanoparticles, and its optical properties. Journal of Materials Science: Materials in Electronics, 28, 7677–7685. https://api.semanticscholar.org/CorpusID:136329759
51. Neena, D., Shah, A. H., Deshmukh, K., Ahmad, H., Fu, D. J., Kondamareddy, K. K., Kumar, P., Dwivedi, R. K., & Sing, V. (2016). Influence of (Co-Mn) co-doping on the microstructures, optical properties of sol-gel derived ZnO nanoparticles. The European Physical Journal D, 70(3), 53. https://doi.org/10.1140/epjd/e2016-50540-5
52. Fei, W., Song, Y., Li, N., Chen, D., Xu, Q., Li, H., He, J., & Lu, J. (2019). Hollow In2O3@ZnFe2O4 heterojunctions for highly efficient photocatalytic degradation of tetracycline under visible light. Environmental Science: Nano, 6(10), 3123–3132. https://doi.org/10.1039/C9EN00811J
53. Rafaie, H. A., Nor, R. M., & Amin, Y. M. (2015). Magnesium doped ZnO nanostructures synthesis using citrus aurantifolia extracts: Structural and field electron emission properties. Materials Express, 5(3), 226–232. https://doi.org/10.1166/mex.2015.1227
54. Alias, S. S., Ismail, A. B., & Mohamad, A. A. (2010). Effect of pH on ZnO nanoparticle properties synthesized by sol–gel centrifugation. Journal of Alloys and Compounds, 499(2), 231–237. https://doi.org/https://doi.org/10.1016/j.jallcom.2010.03.174
55. Ivetic, T. B., Dimitrievska, M. R., Fincur, N. L., Dacanin, L. R., Guth, I. O., Abramovic, B. F., & Lukic-Petrovic, S. R. (2014). Effect of annealing temperature on structural and optical properties of Mg-doped ZnO nanoparticles and their photocatalytic efficiency in alprazolam degradation. CERAMICS INTERNATIONAL, 40(1), 1545–1552. https://www.tib.eu/de/suchen/id/BLSE%3ARN341768962

56. Chaim, T. A., Bernardi, M. I. B., Vicente, F. S. De, Otuka, A. J. G., & Mesquita, A. (2025). Red Shift in Photoluminescence Emissions of ZnO Nanoparticles with Mg Incorporation. 2025 SBFoton International Optics and Photonics Conference (SBFoton IOPC), 1–3. https://doi.org/10.1109/SBFotonIOPC66433.2025.11218576
57. Nisar, A., Saeed, M., Usman, M., Muneer, M., Adeel, M., Khan, I., & Akhtar, J. (2020). Kinetic modeling of ZnO-rGO catalyzed degradation of methylene blue. International Journal of Chemical Kinetics, 52(10), 645–654. https://doi.org/https://doi.org/10.1002/kin.21389
58. Saeed, M., Siddique, M., Ibrahim, M., Akram, N., Usman, M., Aleem, M. A., & Baig, A. (2020). Calotropis gigantea leaves assisted biosynthesis of ZnO and Ag@ZnO catalysts for degradation of rhodamine B dye in aqueous medium. Environmental Progress & Sustainable Energy, 39(4), e13408. https://doi.org/https://doi.org/10.1002/ep.13408
59. Nadumane, A., Shetty, K., Anantharaju, K. S., Nagaswarupa, H. P., Rangappa, D., Vidya, Y. S., Nagabhushana, H., & Prashantha, S. C. (2019). Sunlight photocatalytic performance of Mg-doped nickel ferrite synthesized by a green sol-gel route. Journal of Science: Advanced Materials and Devices, 4(1), 89–100. https://doi.org/https://doi.org/10.1016/j.jsamd.2018.12.002
60. Onotu, O. P., Samuel, H. S., Undie, D. A., Akinpelu, O. O., Ibekwe, F. A., & Etim, E. E. (2025). Nanoparticles for targeted removal of emerging contaminants in wastewater: mechanisms and sustainable practices. Discover Nano, 20(1), 191. https://doi.org/10.1186/s11671-025-04341-4

Received: March 16th 2026 **Accepted: April 22th 2026**